J. Fluid Mech. (1996), *vol.* 321, *pp.* 137–155

Atmospheric solitary waves: some applications to the morning glory of the Gulf of Carpentaria

By LAWRENCE K. FORBES[1] AND SHAUN R. BELWARD[2]

[1] Department of Mathematics, University of Queensland, St Lucia, Queensland 4072, Australia

[2] Department of Mathematics, James Cook University of North Queensland, Townsville 4811, Australia

(Received 7 June 1995 and in revised form 11 March 1996)

A mathematical model is proposed to describe atmospheric solitary waves at the interface between a 'shallow' layer of fluid near the ground and a stationary upper layer of compressible air. The lower layer is in motion relative to the ground, perhaps as a result of a distant thunderstorm or a sea breeze, and possesses constant vorticity. The upper fluid is compressible and isothermal, so that its density and pressure both decrease exponentially with height. The profile and speed of the solitary wave are determined, for a wave of given amplitude, using a boundary-integral method. Results are discussed in relation to the 'morning glory', which is a remarkable meteorological phenomenon evident in the far north of Australia.

1. Introduction

The study of solitary waves in recent decades has been extensive, and a vast literature now exists on the topic. These phenomena are of great importance, not only in fluid mechanics, but also in fundamental physics and optics, for example. A substantial review of much of the earlier work on solitary waves is presented by Miles (1980), who concentrates on approximate theories of the Korteweg–de Vries type. The solitary wave is also discussed briefly in a review article by Schwartz & Fenton (1982), in the context of finite-amplitude surface waves in fluid mechanics.

Much of the earlier work on solitary waves in fluid mechanics made use of weakly nonlinear theories, and an elegant exposition of such a development is given by Stoker (1957). More recently, however, numerical schemes have been devised in which the exact (irrotational or constant vorticity) equations are solved in full, without additional approximation. Hunter & Vanden-Broeck (1983) used an integral equation technique in an inverse plane to obtain irrotational solitary waves of arbitrary amplitude below the maximum. The wave of maximum height possesses a corner at its crest, enclosing an angle of 120°, and cannot readily be computed using general integral equation methods. Hunter & Vanden-Broeck overcame this difficulty by resorting to a power-series type solution in a conformally mapped plane, in which the branch type singularity resulting from the 120° angle at the wave crest was accounted for explicitly in the assumed form of the solution.

Constant vorticity can be accommodated within calculations of the type described above, and has been addressed by several authors, in view of its relevance to shear flows. Benjamin (1962) investigated weakly nonlinear theories, and showed that the value of free-stream speed at which the branch of solitary waves bifurcates from the uniform flow solution is increased by the presence of vorticity. Both periodic and

solitary waves in shear flows were studied by Teles da Silva & Peregrine (1988) using an integral equation technique. They identified limiting waves having an enclosed angle of 120° at the crest, exactly as for irrotational waves, and also suggested that purely rotational waves, in the absence of gravity, might ultimately tend to a limiting form possessing overhanging portions in the free surface, as the wave amplitude becomes infinite; the profile would resemble a circle above a horizontal line. These predictions have been confirmed by Vanden-Broeck (1994), who computed a family of limiting solitary waves for which the vorticity is sufficiently strong to permit infinite amplitude disturbances with large fractions of over-hanging free surface.

Solitary waves at the interface of two fluids are also of interest, and occur both within the ocean and in the atmosphere. Numerical solutions for interfacial solitary waves were computed by Pullin & Grimshaw (1988), using a boundary-integral technique combined with conformal mapping. They also obtained large amplitude configurations close to a limiting form enclosing an angle of 120° at the crest, in addition to waves of unbounded amplitude in the Boussinesq limit as the densities of the two fluids became nearly equal. When constant vorticity was present, and in the Boussinesq limit with zero vorticity, the extreme interfacial waves were again found to possess pronounced overhanging regions.

The situation in the atmospheric is possibly more complex than the oceanographic case, and a simple model of solitary waves occurring at the interface of two homogeneous fluids of different densities may be inappropriate. Indeed, it seems probable that atmospheric solitary waves can form under a variety of circumstances. They are evidently possible within continuously stratified fluids, and have been studied in that case by Miesen, Kamp & Sluijter (1990) and Turkington, Eydeland & Wang (1991), for example. In addition, waves in the atmosphere can form along a pycnocline, which is essentially an interface between two fluids of different densities, since there is a rapid change of density in this region. Such a situation can arise when a cool downdraft from a thunderstorm penetrates beneath the existing stratified atmosphere, and progressive waves in such circumstances have been modelled by Forbes & Belward (1992, 1994). A recent paper by Manasseh & Middleton (1995) gives details of observations of atmospheric waves produced by precisely this mechanism, when a thunderstorm moved past Sydney airport in Australia; an analysis of weakly nonlinear theory led these authors to conclude that the atmospheric waves they observed were, in fact, fully nonlinear.

Perhaps the most spectacular instances of atmospheric solitary waves are the 'morning glory' waves that form in the far north of Australia, on the southern coast of the Gulf of Carpentaria in the state of Queensland. These are remarkable disturbances in the lower atmosphere, which occur in the early morning with considerable regularity during the late spring dry season (September to November) in this remote and inaccessible part of the continent. They are usually accompanied by a wind squall and a striking low cloud formation. Their regularity and clear visibility makes the Gulf of Carpentaria a unique location for the experimental study of these waves, and much work has now been undertaken on them. Results of observations are reported by Smith and Morton (1984), for example, and spectacular photographs of morning glories are given in the papers by Clarke, Smith & Reid (1981), Christie & Muirhead (1983) and Christie (1992). The base of the cloud is about 300 m above ground, and the disturbance moves at 10–20 m s^{-1}. The amplitude of the solitary wave can be at least 1000 m, and the phenomenon is remarkably two-dimensional in appearance, with a long straight crest extending from one horizon to the other. The wave may propagate inland for very great distances, in excess of 300 km, with only

slight change of form. A recent article by Reeder *et al.* (1995) documents an event in which two morning glories interacted over the Gulf of Carpentaria.

It is, of course, the case that large amplitude atmospheric solitary waves exist in regions other than Australia's Gulf of Carpentaria. A solitary wave on the southern coast of Australia, near Adelaide, was detected by Drake (1984), who monitored the migration of insects in the wave using radar observations. Rottman & Einaudi (1993) describe a solitary wave event measured in the United States in 1969 that travelled a very great distance across land, and a phenomenon similar to the morning glory was observed in Oklahoma in 1982, and is described by Haase & Smith (1984).

Much work exists on the modelling of the morning glory phenomenon, and usually involves weakly nonlinear analyses of some type. Christie (1989) considered a Benjamin–Davis–Ono equation and a modification to account for turbulence, and a similar technique is adopted by Rottmann & Einaudi (1993). More recently, some numerical results obtained from a study of Long's equation have been presented by Brown & Christie (1994).

The purpose of the present paper is to develop a fully nonlinear method for modelling atmospheric interfacial solitary waves, using a straightforward integral equation method in primitive variables, similar to that presented by Vanden-Broeck (1994). This method is capable of computing waves of arbitrary amplitude, and it is clear from the observations of morning glory solitary waves that the amplitude may exceed the depth of the lower fluid layer, so that highly nonlinear waves are an expected outcome. The original model of Forbes & Belward (1992) is used to describe the morning glory, and consists of a layer of cool, incompressible air moving beneath a stationary atmosphere that is compressible and isothermal. In addition, shear is included in the moving lower layer, as a simple model of the interaction of the fluid in this layer with the ground.

2. The two-fluid model

We consider a two-fluid system, in which cool, essentially incompressible air is moving beneath a stationary compressible atmosphere. A Cartesian coordinate system (X, Y) moves with the wave, so that the flow is steady in this moving frame. The X-axis is located along the horizontal ground, and the Y-axis points vertically (in the opposite direction to the acceleration g due to gravity), and the solitary wave is assumed to be symmetrical about the Y-axis. The upper, compressible fluid will be referred to as layer 1, while the lower incompressible air will be denoted as layer 2. There is assumed to be a sharp interface between the two fluid layers, at height H above the ground, far from the wave.

In the upper fluid (layer 1), the stationary air is assumed to be isothermal, with temperature T_0 and universal gas constant R. It follows from the ideal gas law and the hydrostatic pressure condition that the density and pressure in this upper layer have the well-known exponential forms

$$\left.\begin{aligned} \rho_1(Y) &= A_1 \exp\left(-\frac{gY}{RT_0}\right), \\ p_1(Y) &= RT_0 A_1 \exp\left(-\frac{gY}{RT_0}\right), \end{aligned}\right\} \tag{2.1}$$

where the symbols ρ and p represent density and pressure, respectively, and A_1 is a constant with a value yet to be determined. In reality, the upper layer 1 would be in

motion to some extent, instead of being completely at rest, as is assumed here; nevertheless, the work of Forbes & Belward (1994) indicates that this is unlikely to affect the results obtained here, for most physically realizable wind speeds in upper layer 1. Consequently, the assumption of a stationary upper fluid is expected to be adequate.

The lower fluid in layer 2 is assumed to be in motion, perhaps as the result of a distant thunderstorm, or else due to sea breezes in the case of the morning glory phenomenon. At ground level, the horizontal wind speed (relative to the moving wave-based coordinates) is c, but friction effects in this narrow ground layer give rise to a vorticity distribution which is assumed to be constant, for the sake of simplicity, and of magnitude ω. Far from the wave, the velocity vector $\boldsymbol{q}_2 = u_2\boldsymbol{i} + v_2\boldsymbol{j}$ therefore has horizontal component $u_2 \to c + \omega Y$ and vertical component $v_2 \to 0$, as $X \to \pm\infty$. At each point in lower fluid 2, the vorticity is thus curl $\boldsymbol{q} = -\omega\boldsymbol{k}$, where the symbols $\boldsymbol{i}, \boldsymbol{j}$ and $\boldsymbol{k}$ represent the three unit vectors in the directions of the X-, Y- and Z-axes, respectively.

The assumption of constant vorticity in the lower layer is an approximation to the true situation, and it has the advantage of affording a considerable analytical simplification in the calculations. In measurements of pre-glory wind velocity components reported by Smith (1988), it is evident that the horizontal wind speed does indeed have an approximately linear profile up to about 300 m height, with the direction of flow towards the approaching disturbance (so that $\omega > 0$). However, above 300 m, a linear speed profile ceases to apply, and it is even possible for flow reversal to occur. Thus for the morning glory wave, the structure of the background shear flow may not necessarily be due solely to friction effects in the moving lower layer. Nevertheless, it will be seen that the assumption of a linear profile $u_2 \to c + \omega Y$ ahead of the wave enables us to account for important morning glory effects, such as the rolling that is observed within the wave, as well as the low-altitude wind shear associated with it. Christie & Muirhead (1983) and Smith (1988) identify this wind shear as a significant hazard to aircraft.

Following Forbes & Belward (1992), it is convenient to define the pressure P_A at ground level, far from the wave. Thus $p_2(X, Y) \to P_A$ as $X \to \pm\infty$ and $Y \to 0$. In other words, the quantity P_A would simply be the barometric pressure measured by an observer on the ground either long before or long after the morning glory event had passed overhead. From Euler's equation of motion, it follows that the pressure in lower layer 2 far from the wave has the hydrostatic form

$$p_2(X, Y) \to P_A - \rho_2 g Y \quad \text{as} \quad X \to \pm\infty, \tag{2.2}$$

in which ρ_2 is the (constant) density in layer 2. At these great distances from the solitary wave crest, the interface between layers 1 and 2 becomes horizontal, with $Y \to H$, and the dynamic condition that the two pressures p_1 and p_2 in (2.1) and (2.2) should be equal on the line $Y = H$ then yields the constant A_1 in (2.1) as

$$A_1 = \frac{P_A - \rho_2 g H}{RT_0} \exp\left(\frac{gH}{RT_0}\right). \tag{2.3}$$

Although the fluid in lower layer 2 is flowing rotationally, it is nevertheless possible to integrate Euler's equations of motion once, to yield a Bernoulli equation of the type

$$\tfrac{1}{2}(u_2^2 + v_2^2) + p_2/\rho_2 + gY = C, \tag{2.4}$$

in which C is a constant on any particular streamline, but may vary across streamlines. Now the interface itself is a streamline, and equating the pressure p_2 at the interface to

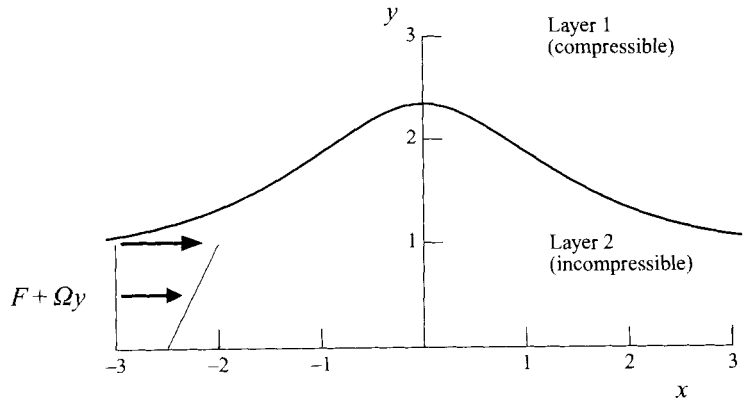

FIGURE 1. A sketch of the flow configuration in dimensionless coordinates. The interface is taken from a portion of an actual solution for an atmospheric interfacial solitary wave, with parameters $\alpha = 0.05$, $\beta = 20$, $\Omega = 0.2$. The wave is close to the maximum, and has amplitude $A = 1.35$, with computed ground speed $F \approx 0.2981$. (In dimensional variables with interface height $H = 400$ m, computed speed $c \approx 19$ m s^{-1}). The scale on both axes is the same.

pressure p_1 there, as given by (2.1) and (2.3), the Bernoulli condition (2.4) at the interface becomes

$$\tfrac{1}{2}(u_2^2+v_2^2)+\left(\frac{P_A}{\rho_2}-gH\right)\exp\left(\frac{g(H-Y)}{RT_0}\right)+gY=\tfrac{1}{2}(c+\omega H)^2+\frac{P_A}{\rho_2} \quad \text{on interface.} \tag{2.5}$$

At this point it is convenient to introduce non-dimensional variables and parameters, and these will be used exclusively from now on. All lengths are scaled with respect to the undisturbed depth H of the interface far from the wave, and the quantity $(gH)^{1/2}$ is taken as the reference speed. (Note that our choice of dimensionless variables differs slightly from the usual practice, in which the speed $c+\omega H$ at the interface is taken as the reference dimensional speed; see e.g. Vanden-Broeck (1994). This has the disadvantage that the speed c, which is yet to be determined, appears in combination with the vorticity ω in the formation of a dimensionless parameter, and the influence of the vorticity upon the wave speed is therefore difficult to quantify). With this choice of non-dimensionalization, the atmospheric solitary wave will be seen to depend upon five dimensionless parameters. These are the Froude number $F = c/(gH)^{1/2}$ which is a measure of the horizontal wind speed at ground level, and the vorticity parameter $\Omega = \omega(H/g)^{1/2}$. There is also a parameter $\alpha = (gH)/(RT_0)$ that is effectively a measure of the compressibility of the air in upper fluid layer 1, since it is the ratio of the square of the speed of an infinitesimal disturbance in layer 2 to that in layer 1; if $\alpha \to 0$ then the upper fluid becomes incompressible. This parameter is referred to by Belward & Forbes (1995) as an 'expansion parameter'. The fourth constant $\beta = P_A/(\rho_2 gH)$ indicates the ratio of the pressure at the ground to the hydrostatic pressure due to lower layer 2 alone. Thus $\beta > 1$, and in the limit $\beta \to 1$, the upper fluid is absent. The final parameter in the description of the atmospheric solitary wave is the amplitude A, defined to be the dimensionless height difference in the interface between the crest and the far field. A sketch of a typical flow is given in figure 1.

The velocity components u_2 and v_2 in the lower fluid 2 are now separated into purely rotational and irrotational components by writing

$$u_2 = F+\Omega y+U, \quad v_2 = V, \tag{2.6}$$

in which dimensionless coordinates are denoted as $x = X/H$ and $y = Y/H$, as in figure 1. Since the fluid in layer 2 is incompressible, then $\operatorname{div} \boldsymbol{q}_2 = 0$ and it is therefore possible to define a streamfunction ψ_2 that satisfies this condition identically, by means of the relations

$$u_2 = \frac{\partial \psi_2}{\partial y}, \quad v_2 = -\frac{\partial \psi_2}{\partial x}. \tag{2.7}$$

In addition, the augmented velocity components U and V in the relation (2.6) both satisfy conditions of incompressibility and irrotationality, so that it is possible to define a pseudovelocity potential and streamfunction Φ and Ψ, respectively, by

$$U = \frac{\partial \Psi}{\partial y} = \frac{\partial \Phi}{\partial x}, \quad V = -\frac{\partial \Psi}{\partial x} = \frac{\partial \Phi}{\partial y}. \tag{2.8}$$

The relationship between the true streamfunction ψ_2 and the pseudostreamfunction Ψ in lower fluid 2 is therefore seen to be

$$\psi_2 = Fy + \tfrac{1}{2}\Omega y^2 + \Psi. \tag{2.9}$$

At the ground, the usual impermeability condition

$$v_2 = 0 \quad \text{on} \quad y = 0, \tag{2.10}$$

applies, and at the interface, the vanishing of the normal component of velocity leads to the kinematic boundary condition

$$v_2 = u_2(\mathrm{d}y/\mathrm{d}x) \quad \text{on interface.} \tag{2.11}$$

In dimensionless form, the interfacial Bernoulli equation (2.5) becomes

$$\tfrac{1}{2}(u_2^2 + v_2^2) + (\beta - 1)\,\mathrm{e}^{\alpha(1-y)} + y = \tfrac{1}{2}(F+\Omega)^2 + \beta, \tag{2.12}$$

and an additional condition

$$A = y(0) - y(\infty) \quad \text{on interface} \tag{2.13}$$

defines the wave amplitude.

The unknown interface is now parameterized by means of an arclength s, following Forbes (1985), such that $s = 0$ at the wave crest. The interface profile is therefore sought in the form $(x(s), y(s))$, and it follows that these two functions are related by the arclength condition

$$\left(\frac{\mathrm{d}x}{\mathrm{d}s}\right)^2 + \left(\frac{\mathrm{d}y}{\mathrm{d}s}\right)^2 = 1. \tag{2.14}$$

Because the interface is a streamline, it is straightforward to show, using (2.7), that $\mathrm{d}\psi_2/\mathrm{d}s = 0$ along the interface. Differentiating the relation (2.9) and using (2.8) therefore gives

$$\frac{\mathrm{d}\Psi}{\mathrm{d}s} = -(F + \Omega y)\frac{\mathrm{d}y}{\mathrm{d}s} \tag{2.15}$$

on the interface. The irrotational parts U and V of the velocity components in (2.6) may be expressed in the forms

$$\left.\begin{aligned} U(s) &= x'(s)\,\Phi'(s) + y'(s)\,\Psi'(s), \\ V(s) &= y'(s)\,\Phi'(s) - x'(s)\,\Psi'(s), \end{aligned}\right\} \tag{2.16}$$

on the interface, where use has been made of the relations (2.14) and (2.15).

An integral equation method is now employed, to satisfy the field equations (2.8) and bottom condition (2.10) identically, so that only variables at the free boundary need be considered. This procedure has become standard in recent years, and therefore need only be described briefly here.

The relations (2.8) reveal that the complex quantity $W = U - \mathrm{i}V$ is an analytic function of complex coordinate $z = x + \mathrm{i}y$ in lower fluid 2. Cauchy's integral formula may be applied to this function, around a path consisting of all interface points $(x(t), y(t))$, $-\infty < t < \infty$, except that fixed point $(x(s), y(s))$ which must be by-passed by a semi-circular contour of vanishingly small radius lying in fluid 2, an image free boundary below the level $y = 0$ of the actual ground, and two connecting lines at infinity. Thus

$$\oint \frac{W(z(t))\, z'(t)\, \mathrm{d}t}{z(t) - z(s)} = 0, \tag{2.17}$$

on the path described. By making use of the reflection conditions to eliminate variables on the image free boundary, and exploiting the symmetry of the wave about the y-axis, the imaginary part of Cauchy's integral formula (2.17) eventually yields the integral equation

$$\begin{aligned} \pi U(s) = & \int_0^\infty \frac{\Phi'(t)[y(t) - y(s)] - \Psi'(t)[x(t) + x(s)]}{[x(t) + x(s)]^2 + [y(t) - y(s)]^2} \mathrm{d}t \\ & + CPV \int_0^\infty \frac{\Phi'(t)[y(t) - y(s)] - \Psi'(t)[x(t) - x(s)]}{[x(t) - x(s)]^2 + [y(t) - y(s)]^2} \mathrm{d}t \\ & + \int_0^\infty \frac{\Phi'(t)[y(t) + y(s)] - \Psi'(t)[x(t) + x(s)]}{[x(t) + x(s)]^2 + [y(t) + y(s)]^2} \mathrm{d}t \\ & + \int_0^\infty \frac{\Phi'(t)[y(t) + y(s)] - \Psi'(t)[x(t) - x(s)]}{[x(t) - x(s)]^2 + [y(t) + y(s)]^2} \mathrm{d}t, \end{aligned} \tag{2.18}$$

after use has been made of the relations (2.14) and (2.16). The second integral on the right-hand side is singular in the Cauchy principal valued (CPV) sense. This integral equation (2.18) can be shown to be equivalent to that presented by Vanden-Broeck (1994).

3. Numerical solution

It is possible to develop highly efficient numerical algorithms for the solution of the fully nonlinear problem (2.12)–(2.18), which only solve explicitly for one function, say $y'(s)$, and the Froude number F, with all other quantities determined implicitly. When discretization is carried out using a mesh of N grid points, such schemes solve for a minimal set of N unknown quantities. However, it has been observed here that these schemes are seriously lacking in robustness, for a reason that is still unclear, so that successful iteration to a solution is generally unlikely. By contrast, more inefficient schemes that simply solve for all variables on the free surface simultaneously have been found to be highly stable, and one such method is briefly outlined below; on a mesh of N grid points, it solves for a vector of $3N + 1$ unknown quantities. A method based on a similar philosophy has also been used by Vanden-Broeck (1994).

A mesh of N grid points $s_1, \ldots, s_N$ is placed over an appropriate interval of the interface, with $s_1 = 0$ corresponding to the wave crest and the last grid point s_N chosen to be sufficiently far downstream. An initial guess is made for the vector of unknowns

$$\boldsymbol{u} = [x'_1, \ldots, x'_N; y'_1, \ldots, y'_N; \Phi'_1, \ldots, \Phi'_N; F]^T$$

of length $3N+1$, and this vector is corrected iteratively, using Newton's method to force an error vector $\boldsymbol{E}(\boldsymbol{u})$ to zero. On the basis of this initial estimate, all the other required functions at the interface can now be computed, using (2.15), (2.16) and (2.6). The first N components of the $(3N+1)$-vector $\boldsymbol{E}$ are obtained from the arclength condition (2.14) at the N points $s_1, \ldots, s_N$, and the next $N-1$ components come from the Bernoulli equation (2.12) at the points $s_1, \ldots, s_{N-1}$.

A further $N-1$ conditions to be satisfied result from evaluating the integral equation (2.18) at the $N-1$ half-grid points $s_{j+1/2}, j = 1, \ldots, N-1$, and these form the next $N-1$ components of the error vector $\boldsymbol{E}$. The integrals in (2.18) are evaluated using trapezoidal rule integration, and by placing the singular point $s_{j+1/2}$ midway between the collocation points used in the evaluation of the integrals, the Cauchy principal valued singularity in the second integral cancels, by symmetry, and so can be ignored.

At the wave crest, it is necessary to specify

$$x_1 = 0, \quad y_1 = 1 + A,$$

and thus the remaining three components of the error vector $\boldsymbol{E}$ result from the symmetry condition

$$y'_1 = 0$$

at the wave crest, and the two downstream conditions

$$y_N - 1 = 0, \quad \Phi'_N = 0$$

at the last point s_N.

When $N = 151$ points, it is usually sufficient to choose the last grid point to be $s_N = 15$, and then Newton's method is generally observed to converge within five or six iterations to an accurate solution. As an initial guess to the algorithm for small wave amplitudes A, the soliton solution of Stoker (1957) has usually been employed, in the approximate form

$$F \approx \mathrm{e}^{A/2},$$

$$y(s) \approx 1 + A\,\mathrm{sech}^2(\tfrac{3}{2}\kappa s),$$

$$\Phi'(s) \approx -AF\,\mathrm{sech}^2(\tfrac{3}{2}\kappa s),$$

in which $\kappa = (\frac{1}{3}A)^{1/2}$. Larger amplitude waves, or solutions having large vorticity Ω, are easily obtained by bootstrapping, using a previously computed nonlinear solution for different parameter values as an initial guess.

4. Review of single fluid results

Before presenting results for the new atmospheric interfacial solitary waves, it is useful to review briefly the behaviour of solitary waves on the free surface of a single incompressible fluid layer. This can be done simply in the present model by setting $\alpha = 0$ and $\beta = 1$.

Four wave profiles are shown in figure 2, for vorticity parameter $\Omega = 0.6$, and for increasing wave amplitudes $A = 0.4$, 0.8, 1.2 and $A = 1.54$. As the amplitude A is increased, the solitary wave becomes narrower and more sharply peaked, as is evident from the diagram. The largest wave shown here is close to a fold bifurcation point, in

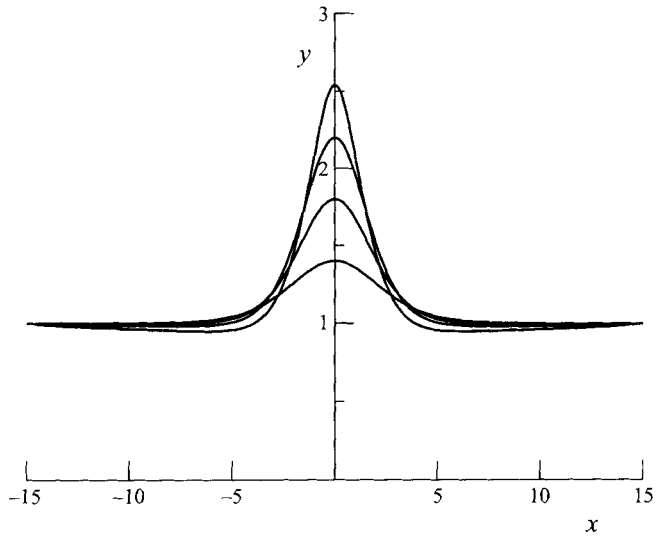

FIGURE 2. Solitary waves for a single fluid layer, $\alpha = 0$, $\beta = 1$, and vorticity $\Omega = 0.6$. Wave profiles are shown for four different values of the amplitude, $A = 0.4, 0.8, 1.2$ and $A = 1.54$ (close to the fold bifurcation in figure 4).

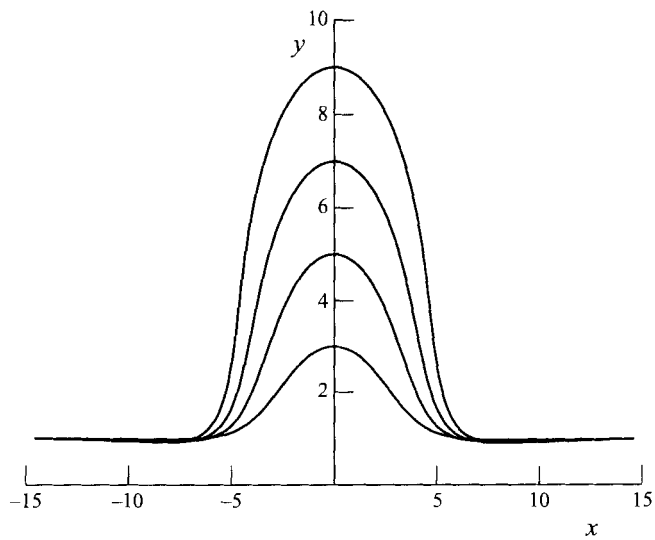

FIGURE 3. Solitary waves for a single fluid layer, $\alpha = 0$, $\beta = 1$, and vorticity $\Omega = 1.4$. Wave profiles are shown for four different values of the amplitude, $A = 2, 4, 6$ and $A = 8$.

the vicinity of which the wave attains both its maximum speed and amplitude; this point will be discussed further later. At this value of vorticity, $\Omega = 0.6$, the branch of solutions is ultimately limited by the formation of a corner at the wave crest, enclosing an angle of 120°, exactly as for periodic gravity waves (see, e.g. Schwartz & Fenton 1982).

Very different behaviour is encountered if the vorticity Ω is sufficiently large, however, and this is illustrated in figure 3 for the case $\Omega = 1.4$ and the four values of wave amplitude $A = 2, 4, 6, 8$. The branch of solitary wave solutions obtained here is now no longer limited by the formation of a corner at the wave crest, and from the

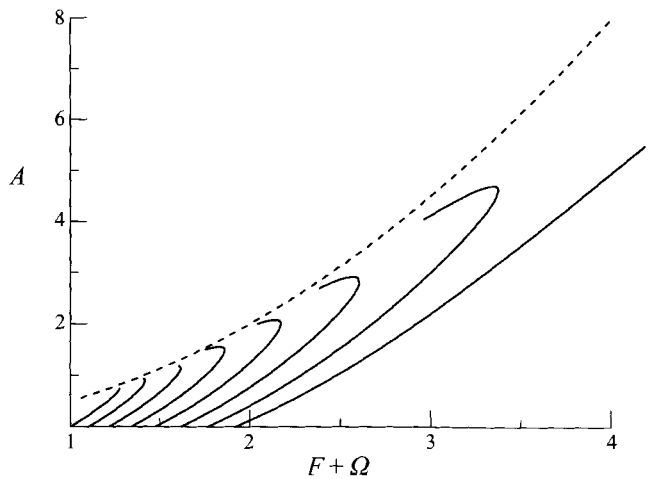

FIGURE 4. Bifurcation diagram for solitary waves on a single fluid layer, $\alpha = 0$ and $\beta = 1$. The dashed line is the locus of limiting waves that possess stagnation points at their crests, which enclose an angle of 120°. Eight bifurcation curves are shown; from left to right the values of vorticity are $\Omega = 0$, 0.2, 0.4, 0.6, 0.8, 1, 1.2 and $\Omega = 1.4$.

mathematical point of view, the amplitude A is free to increase without limit. That this is true for sufficiently large vorticity, even for waves influenced by gravity, was apparently first shown by Vanden-Broeck (1994). As the amplitude A increases, the solitary waves develop a more rounded appearance, owing to the strongly rotating fluid enclosed within the wave, and for sufficiently large amplitude, vertical portions appear on the profile. The wave shown in figure 3, for $A = 8$, is close to the point at which these vertical tangents are formed.

It is presumably the case that solitary waves with vertical sides represent the largest amplitude configurations that would be stable in practice, yet the mathematical solution to (2.12)–(2.18) permits waves of larger amplitude to be obtained. These are known to possess overhanging portions in the profile, so that the wave becomes mushroom shaped, and they persist for arbitrarily large values of amplitude A. Such waves much surely be unstable, as they involve regions of heavy fluid overlying a lighter one, and have therefore not been sought in detail here. Nevertheless, limiting forms of great amplitude for these waves are presented by Vanden-Broeck (1994).

A useful summary of the results for pure solitary waves in single fluid systems may be constructed by means of a bifurcation diagram, in which the Froude number F, computed essentially as a nonlinear eigenvalue of this problem, is shown against the wave amplitude A. Such a diagram is presented in figure 4 for the single fluid case $\alpha = 0$, $\beta = 1$, and has been constructed from the results of approximately 300 separate converged solutions. The amplitude A is shown on the vertical axis, and on the horizontal axis is plotted the dimensionless speed $F+\Omega$ of the wave at the interface.

The dashed line in figure 4 is the curve along which solitary waves have reached their limiting form, with a corner at their crests, enclosing an angle of 120°. This curve may be deduced simply from the Bernoulli equation (2.12) which, for $\beta = 1$, yields

$$A_{\max} = \tfrac{1}{2}(F+\Omega)^2, \tag{4.1}$$

and this follows from the fact that the wave crest has become a stagnation point for this limiting configuration, where $u_2 = v_2 = 0$. Thus solitary wave solutions are not possible in the region of parameter space above this parabolic dashed line in figure 4.

A sequence of bifurcation curves is also shown, for values of the vorticity Ω that increase in uniform increments. The points of intersection of these curves with the horizontal axis have been computed from the formula given by Benjamin (1962), and then continued numerically to larger amplitudes. From left to right, the eight curves (sketched with solid lines) correspond to $\Omega = 0, 0.2, 0.4, 0.6, 0.8, 1, 1.2$ and 1.4. When shear is absent in lower fluid layer 2, $\Omega = 0$, there is an increase in interfacial speed $F+\Omega$ with the wave amplitude A, until the limiting wave is formed with a corner at the crest. For small values of $\Omega > 0$, this pattern is repeated, except that a small fold bifurcation is evident, so that the fastest solitary wave for a given vorticity Ω occurs before the maximum height is attained. For larger values of Ω, this fold bifurcation is present, but considerably more pronounced, to the extent that at $\Omega = 1.2$ there is a large interval of wave speeds for which two solitary waves of different height are possible, and the solitary wave evidently achieves both its maximum height and speed in a neighbourhood of the fold. The limiting form, with the corner at its crest, is neither the largest nor the fastest wave that can form when $\Omega = 1.2$. The results shown for $\Omega = 1.2$ (the penultimate curve to the right of figure 4) represent the largest value of vorticity Ω at which the bifurcation curve undergoes this fold; in this case the accuracy of the numerical method becomes slightly unreliable as the curve approaches the limiting form (dashed line), and has not been pursued further.

The last curve on the far right of figure 4 has been obtained with vorticity $\Omega = 1.4$, and its behaviour is qualitatively different to curves obtained at lower values of Ω. It neither undergoes a fold bifurcation nor does it ever approach the limiting curve sketched with a dashed line on the diagram. Thus, when $\Omega = 1.4$, the curve continues indefinitely, so that waves of arbitrarily large amplitude A are possible, at least as mathematical solutions. Some of these have been illustrated in figure 3, and as A increases, it is eventually the case that overhanging portions develop in the wave profiles. Of course, such waves are unlikely to be stable to small perturbations in a fully time dependent calculation.

This concludes the review of results for the single fluid solitary wave, obtained with $\alpha = 0$ and $\beta = 1$. These results essentially constitute a summary of solutions obtained by Vanden-Broeck (1994) for free-surface solitary waves, although we use the quantity $(gH)^{1/2}$ as the dimensional reference speed for the waves. By contrast, Vanden-Broeck makes use of the unknown phase speed c in his unit of speed, and this quantity is then involved in the formation of his vorticity parameter. In fact, the relationship between Vanden-Broeck's vorticity ω_V and inverse Froude number squared G_V and our parameters Ω and F is

$$\omega_V = \frac{\Omega}{F+\Omega}, \quad G_V = \frac{1}{(F+\Omega)^2}.$$

We believe the parameter choice in the present paper to be more natural, in the sense that the Froude number F and vorticity parameter Ω defined here are genuinely independent, but the disadvantage is that a direct comparison with Vanden-Broeck's results is now somewhat difficult. Nevertheless, estimates based on figure 2 in Vanden-Broeck (1994) indicate quantitative agreement between our results and his.

5. Interfacial solitary waves in the atmosphere model

When $\alpha > 0$ and $\beta > 1$, the model of §2 represents the situation of major interest in this paper, in which an incompressible fluid layer moves beneath a stationary compressible atmosphere, and a solitary wave forms along the interface. This is

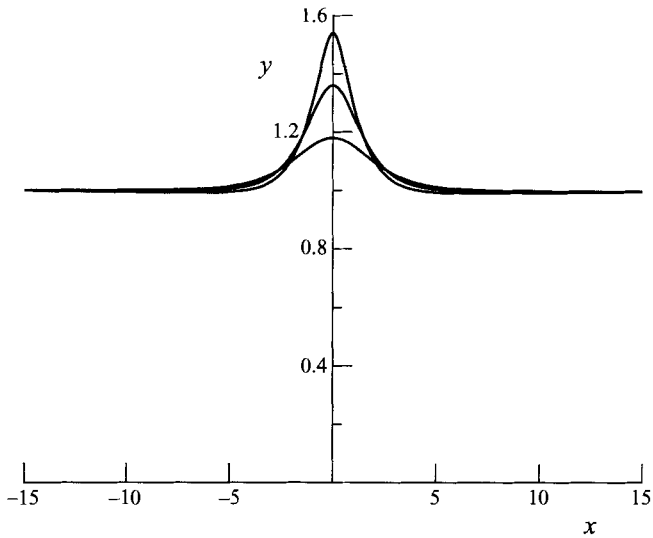

FIGURE 5. Atmospheric interfacial solitary waves, for $\alpha = 0.05$, $\beta = 20$, and vorticity $\Omega = 0$. Wave profiles are shown for three different values of the amplitude, $A = 0.18$, 0.36 and $A = 0.54$.

evidently the condition leading to the morning glory of the Gulf of Carpentaria in Australia's far north, where morning sea breezes penetrate far inland. Notice that, far from the wave crest, the density jump across the asymptotically flat interface is

$$\Delta\rho = \alpha(\beta - 1) - 1, \tag{5.1}$$

and this must be negative if a physically meaningful result is to be achieved, in which lighter fluid overlies heavier fluid.

A great number of numerical solutions has been generated, and bear substantial similarities to the single fluid case discussed in §4. In this section, we present detailed results for the case $\alpha = 0.05$, $\beta = 20$, since these parameter values are representative of the conditions pertaining to the morning glory phenomenon in this model, and satisfy the physical requirement that the density jump $\Delta\rho$ in expression (5.1) must be negative. (In fact, since $\Delta\rho$ is a small quantity, it follows that β must be chosen to be only slightly less than $1 + 1/\alpha$.)

Figure 5 shows three wave profiles for this case $\alpha = 0.05$, $\beta = 20$, for a situation in which there is no shear in the lower fluid layer 2, $\Omega = 0$. In this diagram, the wave amplitudes are $A = 0.18$, 0.36 and 0.54, and the largest of these is close to the wave of maximum height, at which a corner stagnation point enclosing an angle of 120° forms at the wave crest. The computed Froude numbers for these three wave profiles are respectively 0.2490, 0.2720 and 0.2901; in dimensional variables, with the interface height chosen to be $H = 400$ m, which is consistent with the observations for the morning glory in the Gulf of Carpentaria, these Froude numbers correspond to wave speeds of 15.6, 17.0 and 18.1 m s^{-1}, and these are all within the measured range for morning glories. Note that, since shear is absent in the lower layer 2 for these results, the horizontal wind speed at the interface is the same as the speed along the ground.

The effect of increasing shear in the lower layer is examined in figure 6(*a*), which shows three atmospheric solitary wave profiles for the case $\alpha = 0.05$, $\beta = 20$ and vorticity $\Omega = 0.4$, and wave amplitudes $A = 0.8$, 1.6 and 2.4. The largest of these waves, obtained with $A = 2.4$, is close to a point of fold bifurcation at which the wave attains a maximum speed, as will be seen later in this section. At this value $\Omega = 0.4$ of

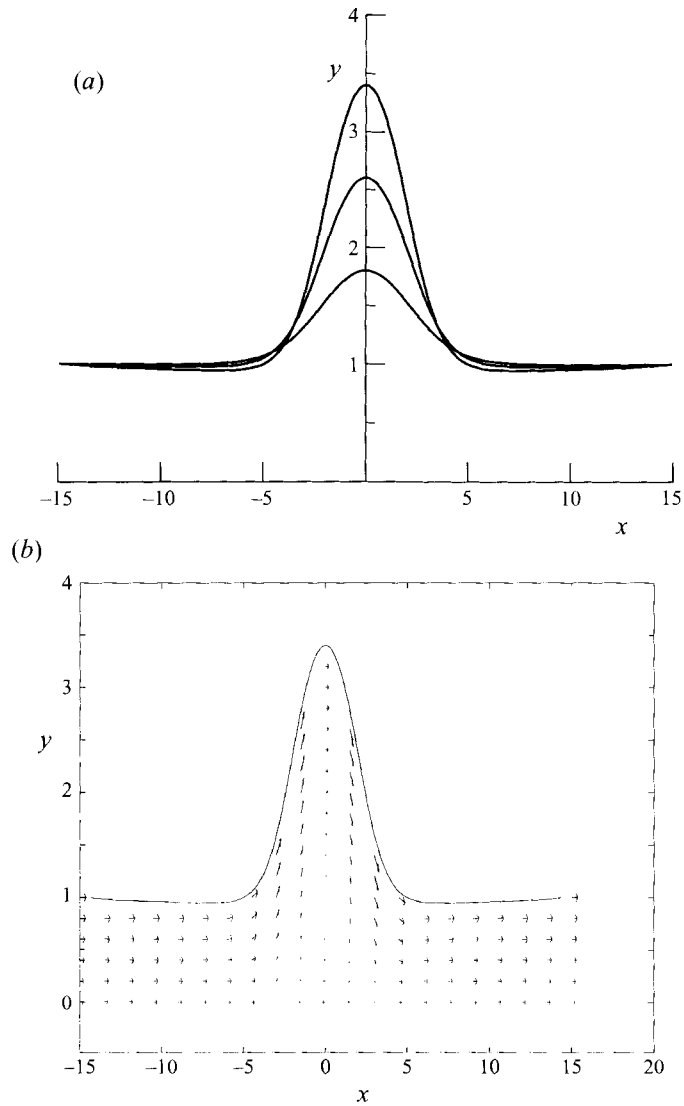

FIGURE 6. Atmospheric interfacial solitary waves, for $\alpha = 0.05$, $\beta = 20$, and vorticity $\Omega = 0.4$. (*a*) Wave profiles for three different values of the amplitude, $A = 0.8$, 1.6 and $A = 2.4$. (*b*) Internal flow structure for the solution with amplitude $A = 2.4$.

the vorticity parameter, the solution branch of solitary waves is again ultimately limited by a configuration that has a corner stagnation point at its crest.

On the basis of the wave speeds computed for the profiles shown in figure 6(*a*), it seems likely that the value $\Omega = 0.4$ would represent the practical upper limit for shear in the lower layer, at least for solitary waves produced by a sea-breeze mechanism, as is the case for the morning glory in Australia. The three Froude numbers corresponding to the amplitudes $A = 0.8$, 1.6 and 2.4 shown in figure 6(*a*) are $F = 0.2421$, 0.3624 and 0.4579, and these give horizontal speeds of approximately 15.2, 22.7 and 28.7 m s^{-1} at ground level, respectively, assuming an interface height $H = 400$ m above ground. Only the first of these, obtained for the wave of amplitude $A = 0.8$ gives a wave speed comparable with measured values, but even in this case, the speed at the interface,

$F+\Omega$, increases to a value which in dimensional terms is approximately 40 m s^{-1} (owing to the presence of the shear), and this apparently lies outside the measured range.

On the basis of the computed wind speeds at $\Omega = 0.4$, it would therefore appear that none of the waves in figure 6(*a*) would correspond to an observed outcome for the morning glory solitary waves. However, the range of amplitudes (up to 2.4 times the depth of the moving lower layer) are within measured values. It is nevertheless possible that waves similar to these might perhaps result from a more violent meteorological event, such as the downdraft from a severe thunderstorm, for example; a recent article by Davies-Jones (1995) shows the way in which an intense, energetic thunderstorm can produce rain-cooled downdrafts (and their role in tornado formation is discussed).

In figure 6(*b*), the internal flow is shown for the largest wave in figure 6(*a*), obtained with $\alpha = 0.05$, $\beta = 20$, $\Omega = 0.4$ and amplitude $A = 2.4$. The horizontal and vertical velocity components u_2 and v_2 (in a coordinate system moving with the wave) were computed using Cauchy's integral formula to obtain the irrotational parts U and V, and then calculating u_2 and v_2 from (2.6). In fact, the formula for U within the wave is the same as (2.18), except that the interfacial coordinates $x(s), y(s)$ are replaced with an internal point (x, y), and the term $\pi U(s)$ on the left-hand side of (2.18) is replaced with $2\pi U$. A similar expression for V is obtained by taking the real part of (2.17).

Figure 6(*b*) shows that, for waves of large amplitude, the vorticity Ω causes a re-circulating region of flow to form beneath the wave crest. This is consistent with Smith's (1988) observations of the rolling within a morning glory wave. Associated with this phenomenon are strong downdrafts that would be experienced soon after the crest of the wave had passed an observer on the ground. These would certainly pose a wind-shear threat to low-flying aircraft.

As with solitary waves on a single fluid layer, investigated in §4, the present atmospheric model also permits waves of arbitrarily large amplitude to form if the vorticity Ω is suitably large. To illustrate such waves, we present four profiles obtained with $\Omega = 0.8$, and amplitudes $A = 2$, 4, 6 and 8 in figure 7(*a*). These are similar to the single fluid results displayed in figure 3, although the crests are rather broader. The largest of these waves, obtained with $A = 8$, is again close to a configuration having vertical sections in the profile; larger waves possessing overhanging sections are a theoretical possibility, but would presumably be unstable owing to the fact that portions of the heavier, incompressible fluid for layer 2 would then overlie lighter, compressible fluid from layer 1, and no attempt has been made to compute such waves here. As indicated above, it is highly unlikely that atmospheric solitary waves similar to those in figure 7(*a*) would be observed at all, in view of the very large vorticity $\Omega = 0.8$ required to produce them, and so these results have been presented purely for completeness.

A plot of the internal flow within the largest of the waves in figure 7(*a*) is given in figure 7(*b*). Here, the amplitude is $A = 8$ and the other parameters are $\alpha = 0.05$, $\beta = 20$ with vorticity $\Omega = 0.8$. The velocity components u_2 and v_2 were computed from the known interface profile using Cauchy's integral formula, as explained in the discussion of figure 6(*b*), and clearly show a pronounced region of rotating flow within the wave crest. Close behind the crest is a region of very severe downdraft, associated with the re-circulation in the crest. It is unlikely that an atmospheric solitary wave of such large amplitude would be encountered in practice, and so the extreme low-level wind shears shown in figure 7(*b*) are fortunately not likely to be of concern.

We conclude this section with a summary bifurcation diagram, showing the relations between the computed wave speeds and the amplitudes, for five different families of

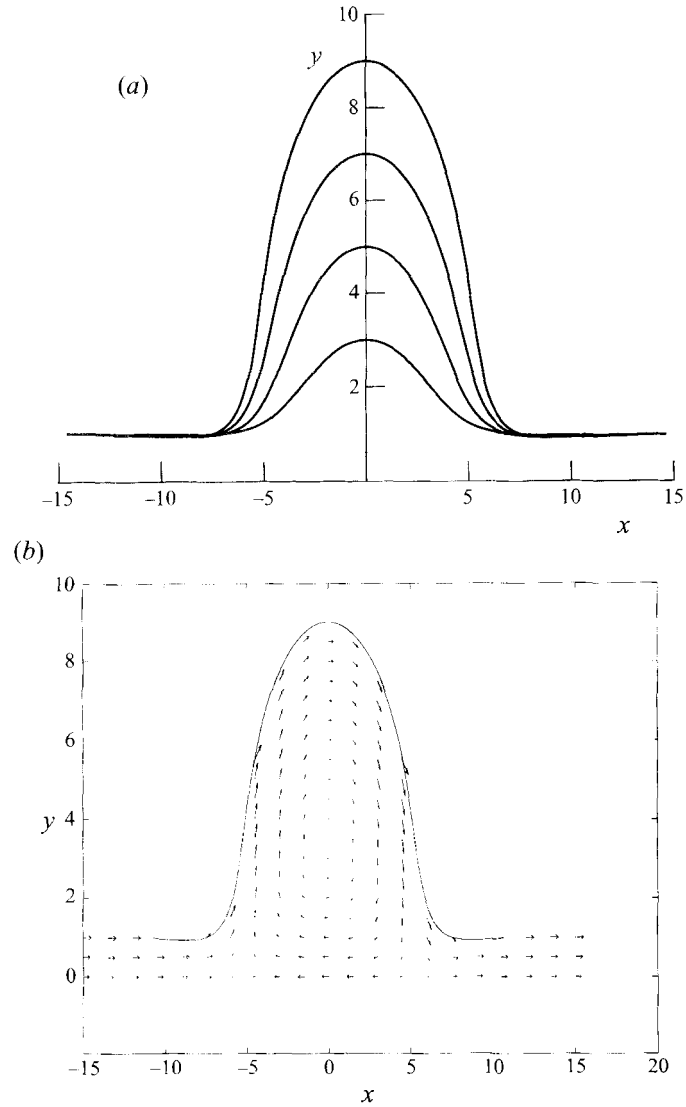

FIGURE 7. Atmospheric interfacial solitary waves, for $\alpha = 0.05$, $\beta = 20$, and vorticity $\Omega = 0.08$. (*a*) Wave profiles for four different values of the amplitude, $A = 2$, 4, 6 and $A = 8$. (*b*) Internal flow structure for the solution with amplitude $A = 8$.

waves corresponding to five different values of the vorticity parameter Ω. Figure 8(*a*) shows results for the horizontal wind speed $F+\Omega$ at the interface, and the speed F along the ground is illustrated in figure 8(*b*).

The dashed line in figure 8(*a*) is the locus of limiting solitary waves, for which a corner enclosing an angle of 120° is formed at the crest. It has been obtained by setting velocities to zero in the Bernoulli equation (2.12), and hence determining that

$$(F+\Omega)_{max} = [2A + 2(\beta - 1)(e^{-\alpha A} - 1)]^{1/2}. \tag{5.2}$$

This expression (5.2) reduces to the previous formula (4.1) in the single fluid limit $\beta \to 1$. Solitary waves are not possible in the region above this dashed line in figure 8(*a*).

Five bifurcation curves have been presented in figure 8(*a*), and are based on the

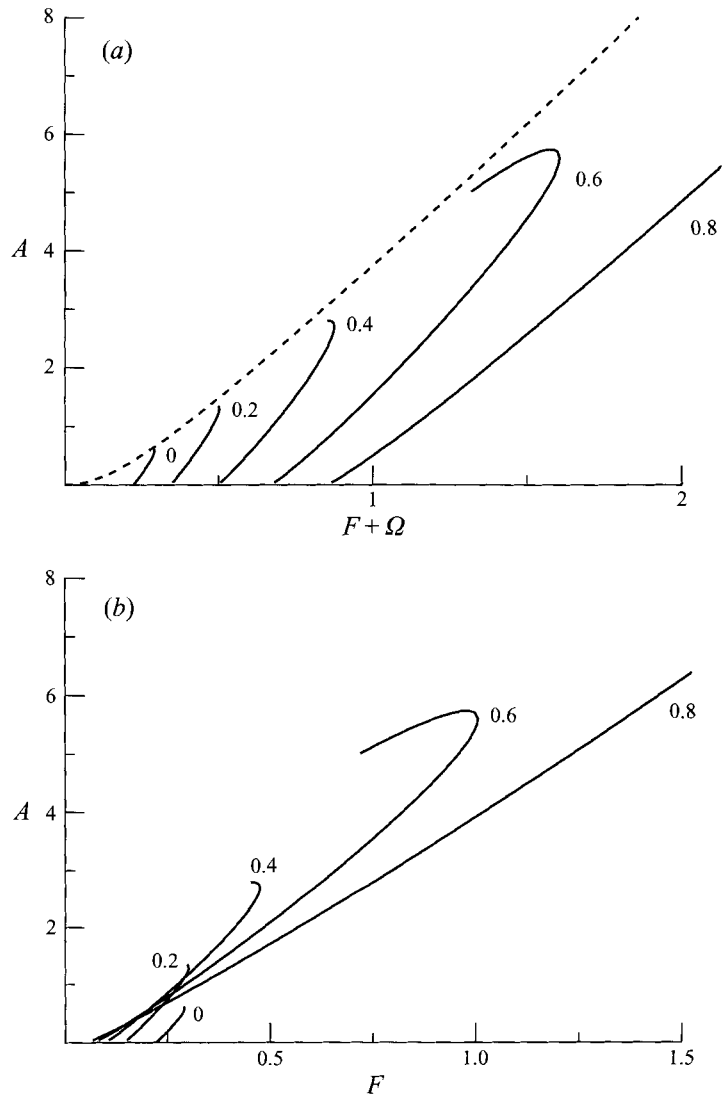

FIGURE 8. Bifurcation diagram for atmospheric interfacial solitary waves, for the case $\alpha = 0.05$ and $\beta = 20$. Five bifurcation curves are shown, for values of vorticity $\Omega = 0$, 0.2, 0.4, 0.6 and 0.8. (*a*) Speed $F+\Omega$ at the interface. The dashed line is the locus of limiting waves that possess stagnation points at their crests, which enclose an angle of 120°. (*b*) Speed F at the ground.

results of over 300 separate converged solutions obtained by the Newton algorithm of §2. From left to right, the curves correspond to vorticities $\Omega = 0$, 0.2, 0.4, 0.6 and 0.8, increased in equal increments. When shear is absent, $\Omega = 0$, the amplitude increases until the limiting configuration is obtained, with its corner stagnation point at the crest. As Ω is increased, a fold bifurcation becomes evident in the curves, so that when vorticity has been increased to $\Omega = 0.6$, the effect of this fold is very strong, with a large overlap region formed, in which two different solitary waves are possible at the same speed. When Ω is increased beyond about $\Omega = 0.6$, the solution branch produced no longer intersects the dashed curve, and in these cases, there is thus no finite limiting wave. A solution branch of this type is shown to the far right of figure 8(*a*), for $\Omega = 0.8$, and at this large value of the vorticity, the solitary waves are free to

increase without limit, eventually forming overhanging portions in their profiles. As indicated above, however, it is unlikely that results for which $\Omega > 0.4$ would ever be observed in practice.

The equivalent diagram for the Froude numbers F is given in figure 8(*b*), so that the horizontal axis corresponds to the air speed at ground level. The fold bifurcations in the solution branches are evident for $\Omega \leqslant 0.6$, but when $\Omega = 0.8$ a different qualitative behaviour is possible, where the wave may in theory increase without limit.

A comparison of the bifurcation diagram figure 8(*a*) for this case with the corresponding picture (figure 4) for the genuine single-fluid case, discussed in §4, shows that the effect of the small compressibility parameter α can indeed be profound. In the single-fluid case, figure 4 shows that, for background vorticity $\Omega = 0.8$ for example, there is a wave of maximum amplitude $A \approx 2.08$. By contrast, it is evident from figure 8(*a*) that, for the same value of vorticity $\Omega = 0.8$, the inclusion of compressibility effects permits the wave to become arbitrarily large. This represents a very dramatic difference between the two theories. Nevertheless, it is unlikely that such large vorticities Ω would be observed frequently in the atmosphere.

6. Conclusions

In this paper, recent results of Vanden-Broeck (1994) for solitary waves in the presence of shear have been extended to a two-layer atmospheric model, in which the lower layer is regarded as incompressible, and the stationary upper fluid is a compressible ideal gas. This is a simple model of interfacial waves in the atmosphere, and was first proposed by Forbes & Belward (1992). The present paper therefore extends the Forbes–Belward work by considering solitary wave formation in such an atmospheric system, and additionally including shear in the lower layer. In a later paper, Forbes & Belward (1994) allowed motion in the upper fluid, but concluded that this had little effect on interface shapes or wave speeds, for upper fluid speeds of magnitudes that would actually be encountered in the present situation. Consequently, the upper fluid is taken to be stationary in the model discussed here. Nevertheless, the characteristic width of interfacial solitary waves may be influenced significantly by the motion in the upper fluid, at least in weakly nonlinear theory, as described by Christie (1992) and Rottman & Einaudi (1993).

It has been found that atmospheric interfacial solitary waves computed by this model are qualitatively similar to solitary waves in a single fluid. When shear in the lower moving fluid is either absent or small, the solitary wave is ultimately limited by the formation of a corner at the wave crest, in which an angle of 120° is enclosed. For large shear, however, such a free-surface stagnation point is prevented from occurring, and consequently, the solitary wave can increase without limit, ultimately forming overhanging portions in its profile. These mushroom-shaped waves would presumably be unstable to small perturbation, and so would not be seen as steady-state structures in the laboratory.

This atmospheric solitary wave model appears to give a plausible qualitative description of the remarkable 'morning glory' waves that are observed in the far north of Australia; spectacular photographs of this phenomenon are to be found in the review paper of Christie (1992). Comparison of the computed wave speeds with measured values for the morning glory wave suggests that our model only retains validity for modest values of the shear in the lower fluid, $\Omega \lessapprox 0.4$, so that the extremely large amplitude overhanging waves that are theoretically possible for large vorticity Ω are in any case unlikely ever to be observable.

It appears that the model proposed in this paper will provide a useful method for the prediction of atmospheric solitary wave amplitudes or speeds. An additional advantage of the present model, which is not shared by Korteweg–de Vries type approximations, is that the internal flow characteristics of the wave can be predicted easily, once the interface has been determined. Such a calculation allows downdraft wind shears to be estimated, for example. This is of interest in the case of the spectacular morning glory effect, but may be of even greater importance in the case of invisible clear-air solitary waves, which, as indicated by Christie & Muirhead (1983), could pose a significant hazard to low-flying aircraft.

In the present work, as in Forbes & Belward (1992, 1994), the upper atmosphere has been assumed to be isothermal, so that exponential decay of pressure and density with height occurs. This modelling simplification has produced plausible morning glory results. Nevertheless, it would be possible to accommodate more complex atmosphere models into the present formulation, and an obvious candidate for future research would be one in which a linear temperature decay region underlies an isothermal atmosphere.

The assumption of constant vorticity Ω permits the numerical solution to be obtained using the powerful methods of complex-variable theory and integral equations. Nevertheless, the measured pre-glory wind profiles of Smith (1988) indicate that the vorticity is only constant in the lowest 300 m or so of atmosphere, and that the vorticity changes sign at higher altitudes. This most probably explains the fact that our model tends to over-estimate the morning glory wave speeds while giving wave amplitudes within experimental values (for appropriate values of Ω). There is limited scope for accounting for this vorticity reversal in the present integral-equation based formulation, and it would be necessary to partition lower fluid 2 into two regions, one with a positive vorticity and the upper region possessing negative vorticity. Two interfaces would then be present in the fluid, and a problem of considerable complexity would result. For more general vorticity distributions, the integral-equation approach would have to be abandoned, and finite-difference or finite-element techniques would be required. Such an investigation is outside the scope of this paper, but the qualitative agreement of the results obtained here with field data would suggest that such an approach is not urgently needed. It is also possible that closer agreement with experiment may be obtained by considering waves in which regions of non-zero vorticity are embedded within an irrotational stream. Such a study is beyond the scope of the present investigation, and is left to future research.

L.K.F. acknowledges with gratitude an SSP programme from the University of Queensland, during which time much of the work presented here was completed. Computing resources were made available through University of Queensland enabling grant R MATHS UEG-7 93, and EPSRC grant GR/J/75258 at the University of Bristol. Collaboration between the investigators has been generously supported by the Mathematics Department at James Cook University. Comments from the (anonymous) referees have been most helpful.

REFERENCES

BELWARD, S. R. & FORBES, L. K. 1995 Interfacial waves and hydraulic falls: some applications to atmospheric flows in the lee of mountains. *J. Engng Maths* **29**, 161–179.

BENJAMIN, T. B. 1962 The solitary wave on a stream with an arbitrary distribution of vorticity. *J. Fluid Mech.* **12**, 97–116.

BROWN, D. J. & CHRISTIE, D. R. 1994 Fully nonlinear solitary waves in the lower atmosphere. *Sixth Conf. on Mesoscale Processes, 18–22 July, Portland Oregon*, pp. 194–196. American Meteorological Society, Boston, MA.

CHRISTIE, D. R. 1989 Long nonlinear waves in the lower atmosphere. *J. Atmos. Sci.* **46**, 1462–1491.

CHRISTIE, D. R. 1992 The morning glory of the Gulf of Carpentaria: a paradigm for non-linear waves in the lower atmosphere. *Austral. Met. Mag.* **41**, 21–60.

CHRISTIE, D. R. & MUIRHEAD, K. J. 1983 Solitary waves: a hazard to aircraft operating at low altitudes. *Austral. Met. Mag.* **31**, 97–109.

CLARKE, R. H., SMITH, R. K. & REID, D. G. 1981 The morning glory of the Gulf of Carpentaria: an atmospheric undular bore. *Mon. Weather Rev.* **109**, 1726–1750.

DAVIES-JONES, R. 1995 Tornadoes. *Sci. Am.* August, 34–41.

DRAKE, V. A. 1984 A solitary wave disturbance of the marine boundary layer over Spencer Gulf revealed by radar observations of migrating insects. *Austral. Met. Mag.* **32**, 131–135.

FORBES, L. K. 1985 On the effects of non-linearity in free-surface flow about a submerged point vortex. *J. Engng Maths* **19**, 139–155.

FORBES, L. K. & BELWARD, S. R. 1992 Atmospheric interfacial waves. *Phys. Fluids* A **4**, 2222–2229.

FORBES, L. K. & BELWARD, S. R. 1994 Atmospheric interfacial waves in the presence of two moving fluid layers. *Phys. Fluids* **6**, 3306–3316.

HAASE, S. P. & SMITH, R. K. 1984 Morning glory wave clouds in Oklahoma: a case study. *Mon. Weather Rev.* **112**, 2078–2089.

HUNTER, J. K. & VANDEN-BROECK, J.-M. 1983 Accurate computations for steep solitary waves. *J. Fluid Mech.* **136**, 63–71.

MANASSEH, R. & MIDDLETON, J. H. 1995 Boundary-layer oscillations from thunderstorms at Sydney airport. *Mon. Weather Rev.* **123**, 1166–1177.

MIESEN, R. H. M., KAMP, L. P. J. & SLUIJTER, F. W. 1990 Long solitary waves in compressible shallow fluids. *Phys. Fluids* A **2**, 359–370.

MILES, J. W. 1980 Solitary waves. *Ann. Rev. Fluid Mech.* **12**, 11–43.

PULLIN, D. I. & GRIMSHAW, R. H. J. 1988 Finite-amplitude solitary waves at the interface between two homogeneous fluids. *Phys. Fluids* **31**, 3550–3559.

REEDER, M. J., CHRISTIE, D. R., SMITH, R. K. & GRIMSHAW, R. 1995 Interacting 'morning glories' over Northern Australia. *Bull. Am. Met. Soc.* **76**, 1165–1171.

ROTTMAN, J. W. & EINAUDI, F. 1993 Solitary waves in the atmosphere. *J. Atmos. Sci.* **50**, 2116–2136.

SCHWARTZ, L. W. & FENTON, J. D. 1982 Strongly nonlinear waves. *Ann. Rev. Fluid Mech.* **14**, 39–60.

SMITH, R. K. 1988 Travelling waves and bores in the lower atmosphere: the 'morning glory' and related phenomena. *Earth-Science Rev.* **25**, 267–290.

SMITH, R. K. & MORTON, B. R. 1984 An observational study of northeasterly 'morning glory' wind surges. *Austral. Met. Mag.* **32**, 155–175.

STOKER, J. J. 1957 *Water Waves*. Wiley Interscience.

TELES DA SILVA, A. F. & PEREGRINE, D. H. 1988 Steep, steady surface waves on water of finite depth with constant vorticity. *J. Fluid Mech.* **195**, 281–302.

TURKINGTON, B., EYDELAND, A. & WANG, S. 1991 A computational method for solitary internal waves in a continuously stratified fluid. *Stud. Appl. Maths* **85**, 93–127.

VANDEN-BROECK, J.-M. 1994 Steep solitary waves in water of finite depth with constant vorticity. *J. Fluid Mech.* **274**, 339–348.